Applied Nanoscience (2019) 9:1417–1426
https://doi.org/10.1007/s13204-019-00983-w

ORIGINAL ARTICLE

Novel Nd-doping effect on structural, morphological, optical, and electrical properties of facilely fabricated PbI_2 thin films applicable to optoelectronic devices

Mohd. Shkir[1] · Mohd Taukeer Khan[2] · S. AlFaify[1]

Received: 9 November 2018 / Accepted: 14 February 2019 / Published online: 14 March 2019

Abstract
Lead iodide is one of the best room temperature radiation detector including applications in solar cell and photodetectors. Herein, we have fabricated the high-quality thin films of pure and Nd:PbI_2 through a simple and cost-effective spin-coating route and investigated their key properties. X-ray diffraction study confirms the growth orientation of all films along *c*-axis/(001) plane and single phase of 2H-PbI_2 Polytypes with the crystallites of size in range of 21–31 nm. Further confirmation of growth and phase was carried out through FT-Raman analysis. EDX and SEM mapping was also carried out to confirm the Nd doping and its homogeneity in the films. SEM provides a clear view on the surface morphology of grown films and grain size was found in the range of 54–71 nm. Optical measurement shows high transparency, i.e., ~ 90% for grown films in visible to NIR region. The direct bandgap is observed to be enhanced with Nd doping from 2.45 to 2.58 eV; however, there is another bandgap which shows reduction with doping from 2.30 to 2.24 eV. This shows the possibility of existence of sub-energy bandgap in PbI_2. The stable value of refractive index is evaluated ~ 2. The value of ε' is found to varies from 4 to 27 in the energy range of 1–2.5 eV. Optical limiting behavior of all films was also studied at two lasers of $\lambda = 532$ nm and 632.8 nm. Moreover, a device fabrication was done for electrical study and found the resistivity increases from 5.14×10^8 Ω-cm for pure to 1.18×10^9 Ω-cm for 5% Nd-doped PbI_2.

Keywords Semiconductor · X-ray diffraction · Vibrational spectroscopy · SEM/EDX · Optical properties · Electrical properties

Introduction

For years, PbI_2 have been extensively studied for radiation detector in all forms like: crystal, films, and nanostructure (Dmitriev et al. 2008; Bhavsar and Saraf 2003; Wang et al. 2017; Tan et al. 2017; Lan et al. 2017). PbI_2 has impressive optoelectrical properties such as wide energy bandgap (2.3–2.5) eV, which enable device to be operated at room temperature, the excellent light absorption coefficient makes it possible to fabricate an ultrathin device, high resistivity of it suppress leakage current, including high chemical stability and well-organized lamellar structure. The most important feature of PbI_2 is its large atomic number ($Z_{Pb} = 82$, $Z_I = 53$), which make it fast and highly sensitive detector (Wang et al. 2017; Liu et al. 2016; Zhong et al. 2016; Zheng et al. 2016). PbI_2 is also a vital material for the active matrix flat panel imagers (AMFPIs) that can be used as detectors for X-ray digital radiography using the direct conversion method (Condeles and Mulato 2011; Street et al. 2002; Mulato et al. 2001; Ahmad et al. 2009; Woo and Kim 2012).

Doping has been extensively used to tune the properties of nanomaterial according to the device requirements (Khan and Almohammedi 2017; Babkair et al. 2015; Khan et al. 2011). Usually, dopants incorporate into the crystal lattice and modify the electronic structure of the host materials.

Electronic supplementary material The online version of this article (https://doi.org/10.1007/s13204-019-00983-w) contains supplementary material, which is available to authorized users.

✉ S. AlFaify
saalfaify@kku.edu.sa

[1] Advanced Functional Materials & Optoelectronics Laboratory (AFMOL), Department of Physics, College of Science, King Khalid University, Abha 61413, Saudi Arabia

[2] Department of Physics, Faculty of Science, Islamic University of Madinah, Madinah, Saudi Arabia

Commonly, Cu, Ag (Rybak 2014; Bhavsar 2012), Fe, Ni (Rybak et al. 2005), Al (Mousa and Al-rubaie 2011), Zn (Bhavsar and Saraf 2003), Cs (Shkir et al. 2017), etc. have been used as dopants in PbI_2. Recently, considerable interest in the rare-earth (RE) ion-doped wide bandgap semiconductors has emerged due to their success in the technologies of lasers, optical fibers, fluorescent lamps, light-emitting displays, bioscience, and imaging (Shkir et al. 2017; Gu et al. 2003; Bünzli et al. 2007; Kenyon 2002). Among the REs metals, trivalent Neodymium (Nd^{3+}) is one of the extensively used element for high power laser applications (Yu et al. 2007). The electronic configuration of Nd () provides a number of important lasing transition including $^4F_{3/2} \rightarrow {}^4I_{9/2}$ (900 nm), $^4F_{3/2} \rightarrow {}^4I_{11/2}$ (1.06 µm) and $^4F_{3/2} \rightarrow {}^4I_{13/2}$ (1.35 µm laser channel) (Liu et al. 2009). Usually, $4f \leftrightarrow 4f$ intra-configurational transition is forbidden in REs ion, but when doped into the wider bandgap semiconductors, these forbidden transitions become partially allowed. Furthermore, these ions act as luminescent centers in the bandgap of semiconductors due to their intra-configurational transitions and abundant energy levels (Kumar et al. 2017; Eliseeva and Bünzli 2010; Auzel 2004; Bünzli and Piguet 2005).

In recent years, PbI_2 gains a new interest as an important precursor material for perovskite solar cells and the performance of these solar cell is competing with the established thin-film photovoltaic technologies such as mc-Si solar cells, CdTe and CIGS (Ono et al. 2018; Mesquita et al. 2017; Saliba 2018; Saliba et al. 2018; Salado et al. 2018). It is expected that the Nd-doping can further improve the performance of perovskite solar cells using down-conversion process (Chen et al. 2012; Lian et al. 2013; Zhang and Huang 2010). Nd induces near-infrared emission about 900 nm; therefore, when a high-energy UV photons absorbed by solar cells, Nd can convert it in to near-infrared lower energy photons, which can be absorbed by the cell and hence improve the device performance.

Previously, a lot of studies have been reported on Nd-doped ZnO and SnO_2, focused on the luminescence, magnetic, electrical, and photo catalytic properties (Bouras et al. 2016; Kumar and Sahare 2012; Rinnert et al. 2012; Shide et al. 2010; Rani et al. 2015; Satpal and Athawale 2018), but the reports on the effect of Nd-doping in PbI_2 thin films are absent. Recently, we have synthesized nanorods and single-crystal nanosheets of pure and Nd-doped PbI_2 using microwave-assisted method and studied their structural, optical, and dielectric properties (Shkir and AlFaify 2017). These preliminary results indicate the Nd-doped PbI_2 as potential material for future photovoltaic devices. Usually, photovoltaic and photodetector devices are made in thin-film configuration. In addition, thin films are having benefit of low temperature crystallization and device size compare to bulk and are easy to integrate in microelectronics. Owing to such tremendous usage of films, it is essential to investigate the optical, electrical, and dielectric properties of Nd-doped PbI_2 material in thin-film configuration.

In this paper, we are reporting the preparation of pure and Nd-doped thin films of PbI_2 using cost-effective spin-coating method. We have used various concentrations of Nd dopants in PbI_2 and investigated the effect of doping concentration on the structural, optical, dielectric, and electrical properties of PbI_2 thin films.

Experimental procedure

About 0.3 gm material from previously synthesized pure nanorods (NRs) and 1, 3, and 5% Nd-doped PbI_2 nanosheets (NSs) by our group (Shkir and AlFaify 2017) was liquefy in 5 ml *N,N*-Dimethylformamide (DMF) at 60 °C with continuous stirring for 30 m. Highly transparent solutions with yellow color were attained and subjected to film deposition by spin-coating technique at a constant rate 3000 rpm for 30 s on well-cleaned glass substrates in single layer. Thickness of deposited films was measured to be ~ 100 nm. The current–voltage (*I–V*) characteristics were recorded in the device configuration shown in the schematic below. For device fabrication, first, we have spin casted the thin film of pure and Nd-doped PbI_2 on pre-cleaned FTO substrates using above method, and then, gold (Au) electrodes were deposited by sputtering method.

All-deposited films on glass substrates were tested by Shimadzu LabX XRD-6000 diffractometer, Japan for structural analysis. FT-Raman spectra were measured for vibrational study and SEM (JSM 6360 LA, Japan) was employed to analyze the surface morphology of the prepared films. The more surface studies were also performed and details are provided as supplementary information.

Absorbance (A), transmittance (T), and reflectance (R) were traced using JASCO V-570, UV–Vis–NIR spectrophotometer over 200–2500 nm wavelength region. Optical limiting behavior of films towards two CW lasers of wavelength, i.e., 532 nm and 632.8 nm, has been studied. *I–V* characteristics of all the prepared devices were recorded on Keithley 4200-SCS system at room temperature.

Results and discussion

Structural and vibrational studies

Figure 1a displays the indexed XRD patterns for pure, 1%, 3%, and 5% Nd-doped PbI_2 films. All films are prefrentially grown along (001) plane and belongs to hexagonal phase of 2H-PbI_2 Polytypes (JCPDS# 7-0235). The measured data for all films were subjected to refinement process to POWDERX software to get their lattice constants and are provided in

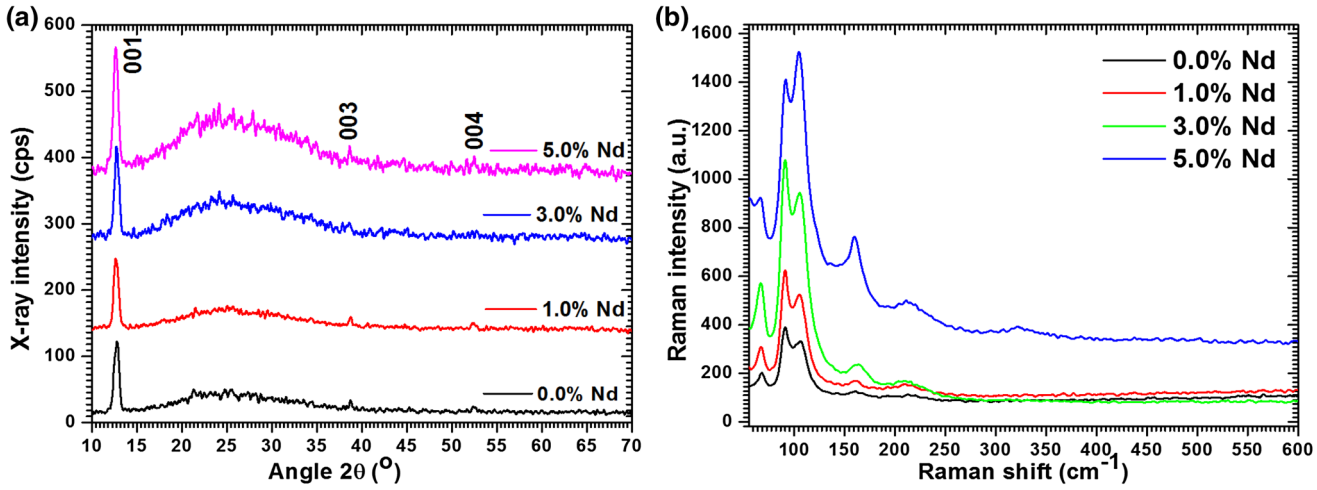

Fig. 1 **a** XRD pattern and (**b**) FT-Raman spectra for Nd:PbI_2 films

Table 1. All parameters are well matched with standard values JCPDS# 7-0235. Tabulated lattice constants are observed to be increased with increase in doping concentration signify the incorporation of Nd in PbI_2 lattice. Similar type of observations was reported previously (Shkir and AlFaify 2017). For evaluating the crystallite size (D), density of dislocation (δ), and strain (ε) values, we need full-width at half-maxima (β) and angular positions (2θ) of peaks which are obtained from XRD-600 software. Using these values, D was calculated from Scherrer's formula (Shkir et al. 2018; AlFaify and Shkir 2019) $\left[D = \frac{0.9\lambda}{\beta \cos\theta}\right]$ and found in range of 21–31 nm. Furthermore, δ and ε values were estimated from (Mohd et al. 2018, 51; Shkir et al. 2017a, b, c) $\delta = 1/D^2$ and $\varepsilon = \frac{\beta \cos\theta}{4}$, respectively, and found in range of 2.6215–4.1621 ($\times 10^{-3}$) nm^{-2} and 1.5695–2.0097, respectively. The value of δ is reducing with increase of crystallite size indicates lessening of defects in grown films. Texture coefficient (TC) was estimated (Shkir et al. 2018) and is tabulated in Table 1, which specify that the TC is large for (001) direction, and hence, films are oriented along (001) plane and 3% Nd:PbI_2 posses larger TC value compare to other films.

The measured FT-Raman spectra of all films are displayed in Fig. 1b which further confirmed their same Polytypic nature and phase in accord to XRD analysis. Raman modes in all films are positioned at ~ 68 ± 2, 91 ± 2, 107 ± 2, 160 ± 2, and 212 ± 2 cm^{-1}, and these modes are showing shift towards lower wavenumber compare to pure as well as reported for bulk crystal (Shkir and AlFaify 2017; Sears et al. 1979; Kasi et al. 2007; Wangyang et al. 2016). As 2H-PbI_2 ought to 3 atoms/unit cell and hence involve 9 degree of vibrations. Out of them two key modes for symmetric stretching, A_{1g} at ~ 97 cm^{-1} and twice degenerated, E_g at 74 cm^{-1} for shearing motion of two I layers (Kasi et al. 2007). However, in the presently grown films, these are positioned at 91 ± 2 and 68 ± 2 cm^{-1}. It can be noticed from these values that they have slight shift owing to transform to nano-dimension crystallites' development in films. The other modes are twice in energy and assigned as overtones to basics modes (Sears et al. 1979).

EDX/SEM mapping, morphological, and roughness analyses

Figure 2 reveals the EDX spectrum and SEM-elemental mapping image for 3 wt.% Nd:PbI_2 film. The existence of Pb, I, and Nd is confirmed in EDX spectrum; moreover, the homogeneous distribution/doping of Nd in PbI_2 is exposed in SEM mapping image. Elemental mapping is one of the good tool to confirm the homogeneity of dopant. Figure 3a–d displays the SEM micrographs for all films which will reveal the effect of Nd doping on surface morphology of films and grain size. SMILE View software was employed to measure

Table 1 Estimated lattice constants, D, δ, ε, and TC values for all Nd:PbI_2 films

Samples	$a = b$ (Å)	c (Å)	V (Å)^3	D (nm)	δ (nm^{-2}) × 10^{-3}	ε × 10^{-3}	$TC_{(001)}$	$TC_{(102)}$
0.0% Nd-PbI_2	4.5537	6.9784	125.3171	22.6435	4.1621	2.0097	3.1536	0.1025
1.0% Nd-PbI_2	4.5550	6.9759	125.3437	21.8876	3.6758	1.9338	3.4152	0.1024
3.0% Nd -PbI_2	4.5565	6.9749	125.4092	30.6130	2.6215	1.5695	4.5351	0.1020
5.0% Nd -PbI_2	4.5594	6.9777	125.6179	25.4875	3.4443	1.8181	3.6487	0.1327

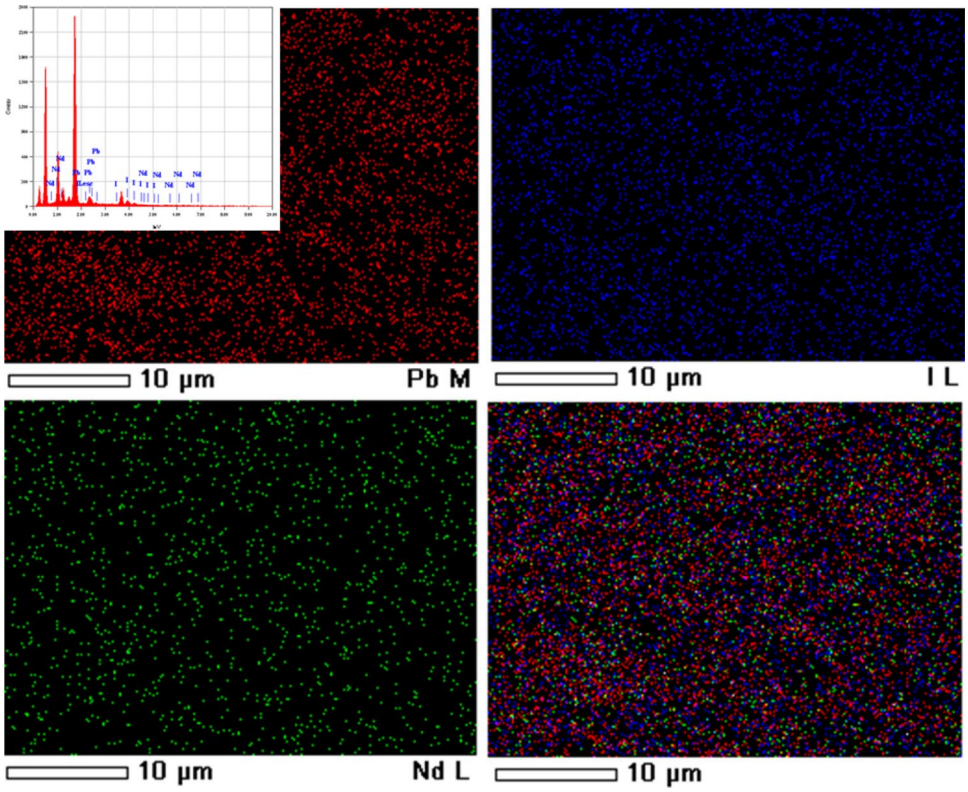

Fig. 2 EDX/SEM mapping image for 3 wt.% Nd:PbI_2 film

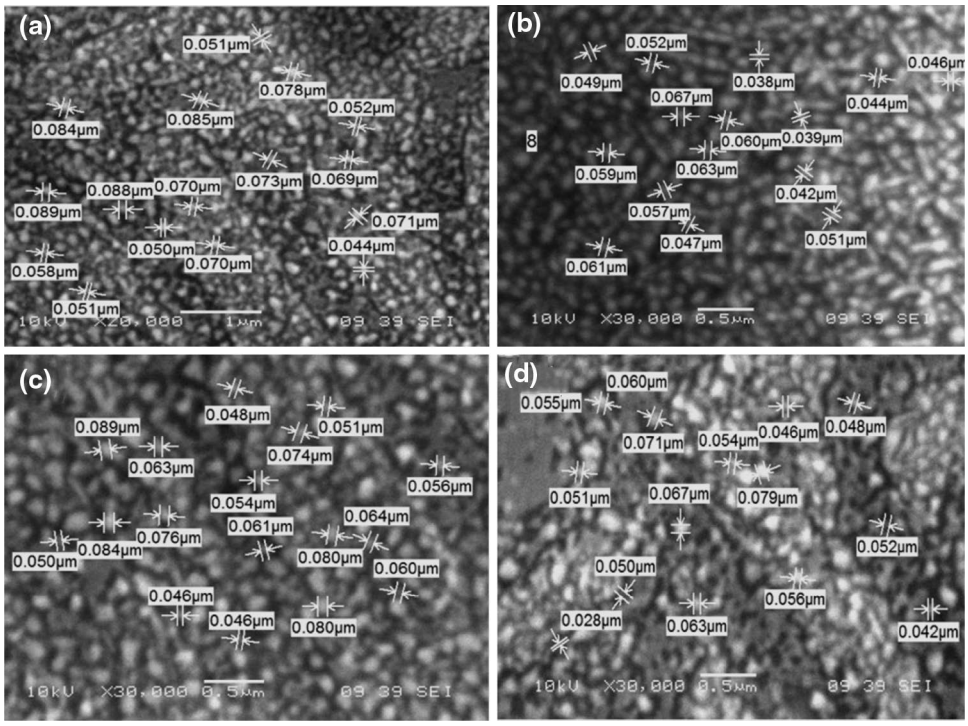

Fig. 3 SEM images for (**a**) 0.0 wt.%, (**b**) 1.0 wt.%, (**c**) 3.0 wt.%, and (**d**) 5.0 wt.% Nd:PbI_2 films

the grain size formed in films. Morphology of the pure PbI_2 film is shown in Fig. 3a, includes nanoparticles of spherical and irregular shapes as well as nanosheets with average grain size of about 71 nm. The spherical nanoparticles along with few nanorods like morphology are revealed in Fig. 3b for 1 wt.% Nd:PbI_2 film and the average grain is reduced to

60 nm. Furthermore, when PbI_2 films were fabricated with 3 and 5 wt.% Nd doping, the morphology reveals spherical nanoparticles of low dimension viz. ~55.5 nm and 54.8 nm, respectively. The grains size attained from SEM images is higher compared to crystallite size (Table 1). The possible reason might be that single grain possess a number of domains of varied orientations that eventually add to bigger size acquire by SEM than XRD. Furthermore, the roughness of films was noticed to be very low (see supplementary data) which is quite comparable with and even less than the previous reports on pure and doped ZnO films (Madhi et al. 2016; Haarindraprasad et al. 2015).

Optical properties

The measured optical A, T, and R spectra are given in Fig. 4a, b; from it, we can notice that the films are showing low absorption and high transmittance values. The *T* value for all films is found in range of 85–90% in visible to NIR region, and such high transmittance indicates that these films can be used as a down shifting converter in solar cells. The absorption edge is noticed to be shifted towards lower wavelength [see inset of Fig. 4a] tends to increase in energy-gap value of films due to Nd doping.

Further, the energy gap (E_g) of all films was evaluated with the help of Tauc's relation: $(\alpha h\upsilon)^{1/n} = A(h\upsilon - E_g)$; here, α is coefficient of absorption, A is constant, h is Plank invariable, and n is associated with transition progression and taken 1/2 for direct bandgap, $E_{g.direct}$. For evaluating $E_{g.direct}$ from the above relation, we have first calculated α from: $\alpha = 2.303\frac{A}{t}$; here, t is thickness. Hence, Tauc's plot is depicted in Fig. 5a as $(\alpha h\upsilon)^2$ (eV.cm^{-1})^2 vs. $h\upsilon$ (eV). In this figure, a line has been drawn to $h\upsilon$ (eV) axis, where $(\alpha h\upsilon)^2 = 0$. and $E_{g.direct}$ have been noted for pure, 1, 3, and 5% Nd-doped PbI_2 films ~ 2.45, 2.47, 2.50, and 2.58 eV, respectively. The calculated $E_{g.direct}$ values are increased by Nd doping and are higher compared to bulk PbI_2 crystals, i.e., 2.27 eV (Zhu et al. 2007). In addition, these bandgaps are much smaller than we have reported for nanostructured (Shkir and AlFaify 2017) and are in close harmony to the prior reports for thin film (Bhavsar and Saraf 2003; Kasi et al. 2007; Caldeira Filho and Mulato 2011; Ghosh et al. 2008). However, there is another sub-energy gap E_g. which shows reduction from 2.30 eV for pure PbI_2 to 2.24 eV for 5% Nd-doped PbI_2.

There are another two fundamental parameters which played important role in photonics devices known as: absorption (k) and refractive (n) indices. These parameters were estimated using the equations: $k = \frac{\alpha\lambda}{4\pi}$ and $n = \frac{(1+R)}{(1-R)} + \sqrt{\frac{4R}{(1-R)^2} - k^2}$ (Shkir et al. 2017) and are revealed in Fig. 5b, c as a function of λ, correspondingly. The k values are showing reduction up to 600 nm, and after that, they becomes almost constant up to NIR region, however, varied with Nd-doping concentrations. The n values are also reducing up to 1200 nm and after that becomes stable. The stable value of n is ~ 2 for all films with minute variation and in accord with the previous one (Buckman et al. 1975).

Dielectric analysis

By keeping in mind about the applications of films as capacitive storage, CMOS, ICs, DRAM, etc. (Panda and Tseng 2013; Ren et al. 2000; Moazzami et al. 1992; Chaneliere et al. 1998), we also investigated the dielectric properties of prepared thin films. The real and imaginary parts of dielectric constant, (ε' & ε'') were evaluated for all films through: $\varepsilon = \varepsilon' + i\varepsilon''$, these parameters gives the idea regarding capacitive and resistivity activities in thin films (Usha et al. 2013). Here, ε' and ε'' were assessed using n

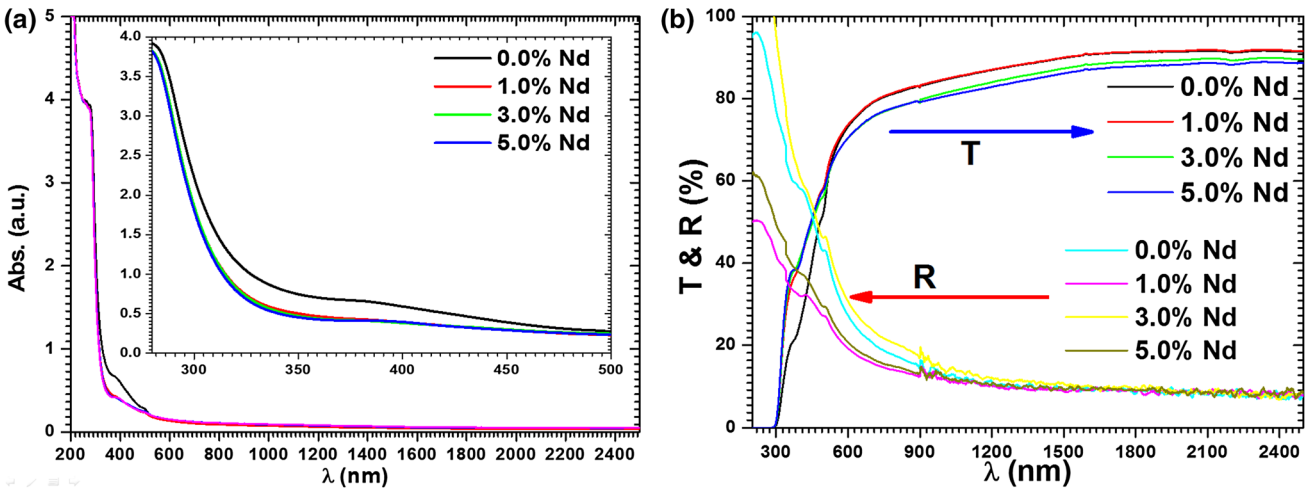

Fig. 4 Spectra for (**a**) Abs. and (**b**) T & R for all Nd:PbI_2 films

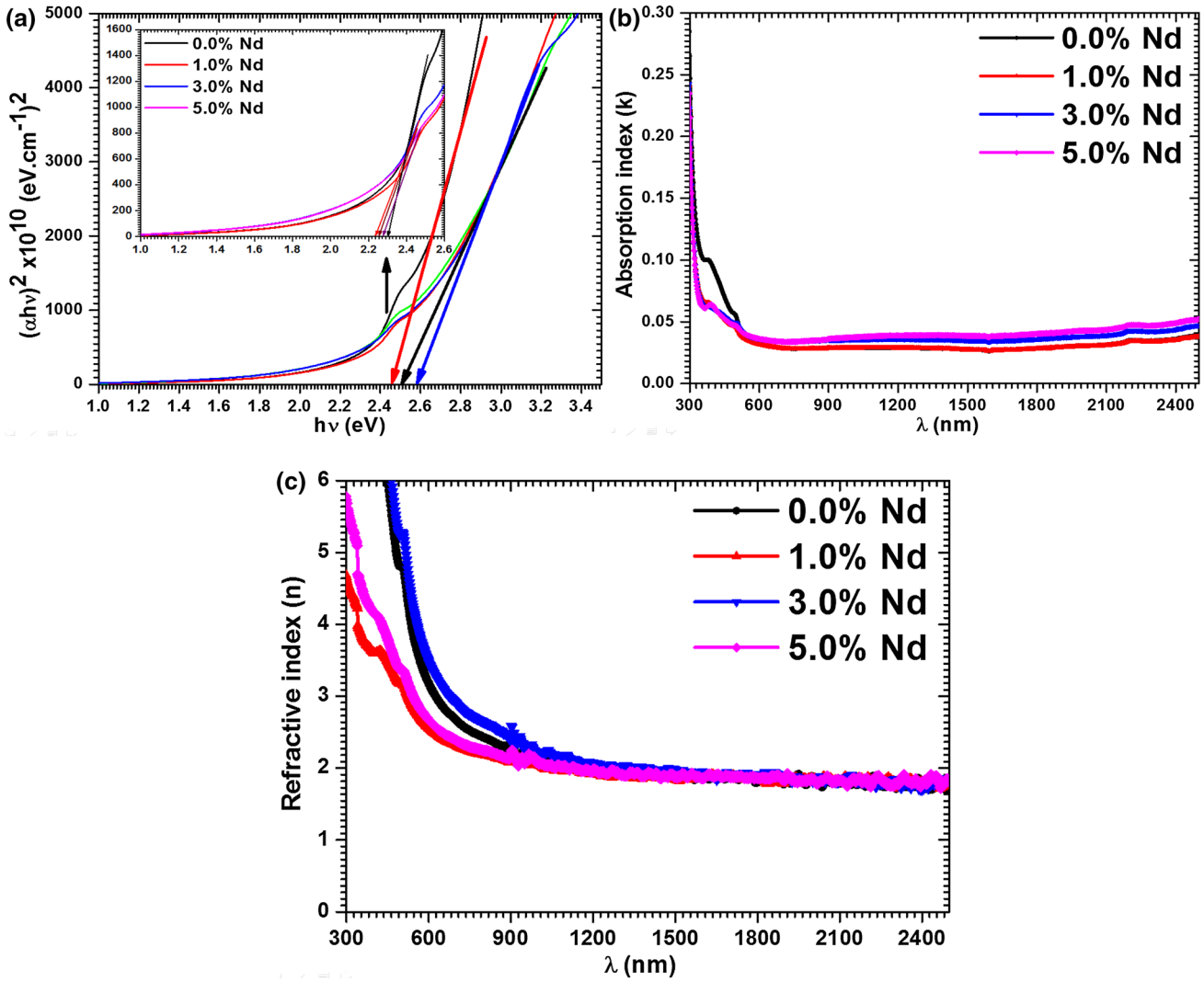

Fig. 5 Plots of (**a**) energy gap, (**b**) *k*, and (**c**) *n* for all Nd:PbI_2 films

and *k* values through (Kim et al. 2012): $\varepsilon' = n^2 - k^2$ and $\varepsilon'' = 2nk$, respectively. The estimated respective values of ε' and ε'' vs. $h\upsilon$ (eV) are plotted in Fig. 6a, b. Figure 6a provides us the value of ε', ~ 4 at low energy, however, with increase of energy, its value increasing, and at 2.5 eV, its value is ~ 23, while at 3.6 eV, it becomes ~ 83 for pure PbI_2 thin film. However, these values reduced to 10 (at 2.5 eV) and 15 (at 3.6 eV) for 1% and 11 (at 2.5 eV) and 21 (at 3.6 eV) for 5% Nd-doped thin films. Moreover, in 3% Nd:PbI_2, these values are higher compared to all other films which are 28 (at 2.5 eV) and 193 (at 3.6 eV). Such variation may be occurred due to various reasons like: films quality, size of grains, disorderness etc. Figure 6b tells the story about ε'' behavior with hυ (eV), and it is noticeable from figure that ε'' has similar behavior to ε' and its value is in range of 0.1–1. The ε'' values are showing the increment with increase of energy for all films. The tanδ values are also revealed in Fig. 6c, which is found in range of 0.01–0.06. Its value is lowest for 3% Nd:PbI_2 films and highest for 1% Nd:PbI_2 films. The low values of tanδ specify that the films are free from foremost defects.

Optical limiting (OL) study

Optical limiters are highly applicable in protecting the optical sensors which are used in link with lasers and arc welders from damaging the light levels (Tutt and Kost 1992; Wood et al. 1989). Owing to such tremendous usage of optical limiters, we have decided to investigate OL behavior of all films using two laser sources of wavelengths viz. 532 nm and 632.8 nm. On incidence of 532 nm (power = 18.5 mW) and 632.8 nm (power = 368.9 μW), the output power from all films was measured through a power meter and is mentioned

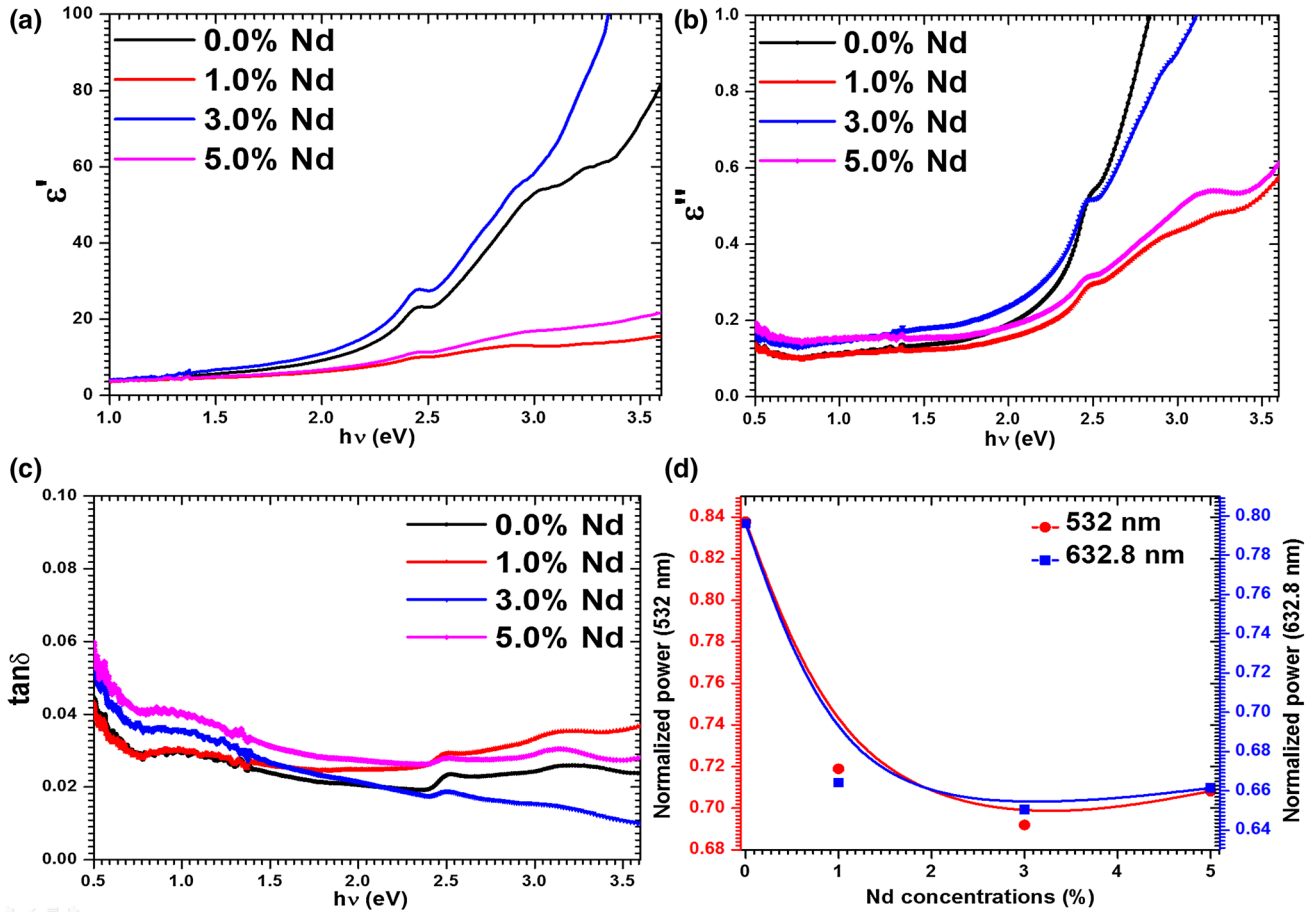

Fig. 6 Plots for (**a**) ε', (**b**) ε'', (**c**) tanδ, and (**d**) optical limiting of all Nd:PbI_2 films

in Table 2 and also depicted in Fig. 6d. From figure, it is revealed that the saturated output power from both the lasers is weaken with increase of Nd-doping in PbI_2. Such behavior signifies that Nd is taking part in alteration of OL conduct of PbI_2 films, owing to change in films quality and crystallinity doped films contains great figure of molecules than pure PbI_2 (Holmen and Haakestad 2016; Poornesh et al. 2010). Therefore, the fabricated films of PbI_2 with Nd-doping will be useful as optical limiters to protect sensor devices from strong lights.

I–V electrical studies

Figure 7 shows the forward and reverse *I–V* characteristics of pure and Nd-doped PbI_2 thin films in the device configuration shown in Scheme 1. It is observed from figure that the current in forward bias is slightly lower than the reverse bias. This is due to higher work functions of anode (Au, 5.0 eV) compared to cathode (FTO, 4.4 eV), indicating that the electron injection is more convenient from FTO than Au. Moreover, the slope of *I–V* curves is 1.2, 1.3, 1.3, and 1.6

Table 2 Optical limiting parameters of Nd:PbI2 films

The input Intensity (I_o)	Thickness	For $\lambda = 532$ nm $I_o = 18.5$ mW		For $\lambda = 632.8$ nm $I_o = 368.9$ μW	
Samples		Output power, (mW)	Normalized power = output power/input power	Output power, (μW)	Normalized power = output power/input power
0.0% Nd:PbI_2	100 nm	15.5	0.83784	293.7	0.79615
1.0% Nd-PbI_2	100 nm	13.3	0.71892	245	0.66414
3.0% Nd -PbI_2	100 nm	12.8	0.69189	240	0.65058
5.0% Nd -PbI_2	100 nm	13.1	0.70811	244	0.66143

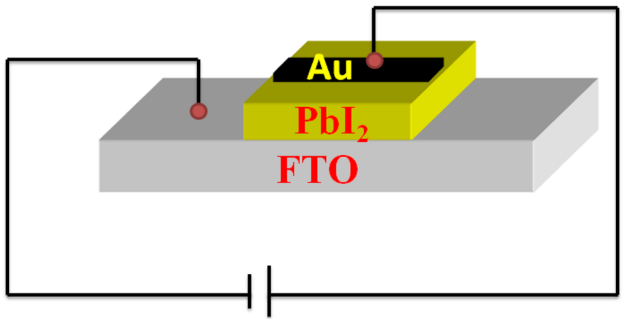

Scheme 1 Schematic of device for *I–V* measurement

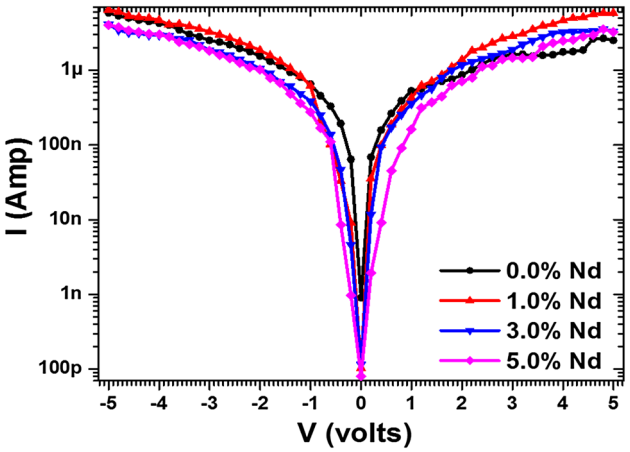

Fig. 7 *I–V* characteristics of pure and Nd-doped thin films

for the Nd-doping concentration of 0%, 1%, 3%, and 5 wt.%, respectively. As the slope of I–V curve of pure PbI_2, thin film is close to 1; thus, ohmic conduction is the dominant charge transport mechanism in these films. The sub-linear relation indicates the presence of traps in the bandgap of semiconductor. Traps are the sub-energy states in the bandgap of semiconductor that limits the motion of charge carriers. Traps are originated from the dislocation or defect present in the crystal structure and also due to the presence of impurities in the materials. The increase of slope with doping concentration is directly related to the increase of trap density in the bandgap of semiconductor. Due to increase of trap density, the charge carriers, who were usually travel to collecting electrodes in pure PbI_2, get trapped to these additional trap states and do not participate in the current and result in decrease of current and increase of resistivity of film. The resistivity of the prepared thin films was calculated from the linear part of the *I–V* curve (0–1 V) through the relation: $\rho = \frac{VA}{Id}$, where A is active area and d is film thickness. The calculated resistivity of prepared thin films are: 5.14×10^8 Ω-cm, 9.52×10^8 Ω-cm, 7.97×10^8 Ω-cm, and 1.18×10^9 Ω-cm for doping concentration of 0%, 1%, 3%, and 5%, respectively. The resistivity of pure film is much smaller than the resistivity of the bulk crystal (10^{13} Ω cm) (Bünzli et al. 2007), and it is comparable to previous value for thin film (Caldeira Filho and Mulato 2011); however, it is about three orders of magnitude smaller than the values obtained by other authors of Refs. (Tan et al. 2017; Kenyon 2002; Yu et al. 2007).

Conclusion

In conclusions, we have prepared the thin films of pure and Nd-doped PbI_2 and investigated their structural, optical, dielectric, and electrical properties. Good crystalline nature and single-phase confirmation for all films was done by XRD and FT-Raman spectra. Crystallite and grain size are of low dimension for all prepared films and also this signify less roughness of films. The prepared thin films show good optical transparency in range of 85–90% which is quite high suggests their applications as a down shifting converter in solar cells. The values of direct bandgap are from 2.45 to 2.58 eV owing to Nd doping. Moreover, additional bandgap observed which shows reduction from 2.30 to 2.24 eV with the increase of Nd-doping concentration. The stable value of *n* is found ~ 2 and ε' value is observed in range of 4–27 and is dependent on energy. The prepared thin films show good optical limiting behavior and can be used to protect the sensor devices from intense light. The resistivity of thin films increases from 5.14×10^8 to 1.18×10^9 Ω-cm for 5% Nd:PbI_2 films, and this might be due to increase of traps in doped PbI_2 thin films.

Acknowledgements The authors would like to express their gratitude to Deanship of Scientific Research at King Khalid University for funding this work through Research Groups Program under Grant No. R.G.P. 1/37/40.

Compliance with ethical standards

Conflict of interest Authors declare that there is no conflict of interest in the current work.

References

Ahmad A, Saq'an S, Lahlouh B, Hassan M, Alsaad A, El-Nasser H (2009) Ellipsometric characterization of PbI2 thin film on glass. Phys B 404:1–6

AlFaify S, Shkir M (2019) A facile one pot synthesis of novel pure and Cd doped PbI2 nanostructures for electro-optic and radiation detection applications. Opt Mater 88:417–423

Auzel F (2004) Upconversion and anti-stokes processes with f and d ions in solids. Chem Rev 104:139–174

Babkair SS, Azam A, Singh K, Dhawan SK, Khan MT (2015) Synthesis and optoelectrical properties of f-graphene/cadmium selenide hybrid system. J Nanophotonics 9:093048

Bhavsar D (2012) Transmittance and reflectance properties of Cu-doped and undoped lead iodide thin films deposited by vacuum evaporation technique. Arch Appl Sci Res 4:1106–1109

Bhavsar D, Saraf K (2003) Optical and structural properties of Zn-doped lead iodide thin films. Mater Chem Phys 78:630–636

Bouras K, Schmerber G, Rinnert H, Aureau D, Park H, Ferblantier G, Colis S, Fix T, Park C, Kim WK (2016) Structural, optical and electrical properties of Nd-doped SnO2 thin films fabricated by reactive magnetron sputtering for solar cell devices. Solar Energy Materials Solar Cells 145:134–141

Buckman A, Hong N, Wilson D (1975) Large refractive-index change in PbI 2 films by photolysis at 150–180 °C, JOSA, 65: 914–918

Bünzli J-CG, Piguet C (2005) Taking advantage of luminescent lanthanide ions. Chem Soc Rev 34:1048–1077

Bünzli J-CG, Comby S, Chauvin A-S, Vandevyver CD (2007) New opportunities for lanthanide luminescence. J Rare Earths 25:257–274

Caldeira Filho AM, Mulato M, Characterization of thermally evaporated lead iodide films aimed for the detection of X-rays, nuclear instruments and methods in physics research section A: accelerators, spectrometers, detectors and associated equipment, 636 (2011) 82–86

Chaneliere C, Autran JL, Devine RAB, Balland B (1998) Tantalum pentoxide (Ta2O5) thin films for advanced dielectric applications. Materials Sci Eng 22:269–322

Chen D, Wang Y, Hong M (2012) Lanthanide nanomaterials with photon management characteristics for photovoltaic application. Nano Energy 1:73–90

Condeles J, Mulato M (2011) Influence of solution rate and substrate temperature on the properties of lead iodide films deposited by spray pyrolysis. J Materials Sci 46:1462–1468

Dmitriev Y, Bennett PR, Cirignano LJ, Klugerman M, Shah KS, PbI2 thick films: Growth, properties, and problems, Nucl Instrum Methods Phys Res Sect A, 584 (2008) 165–173

Eliseeva SV, Bünzli J-CG (2010) Lanthanide luminescence for functional materials and bio-sciences. Chem Soc Rev 39:189–227

Ghosh T, Bandyopadhyay S, Roy K, Kar S, Lahiri A, Maiti A, Goswami K (2008) Optical and structural properties of lead iodide thin films prepared by vacuum evaporation method. Cryst Res Technol 43:959–963

Gu F, Wang SF, Lü MK, Zhou GJ, Liu SW, Xu D, Yuan DR (2003) Effect of Dy3 + doping and calcination on the luminescence of ZrO2 nanoparticles. Chem Phys Lett 380:185–189

Haarindraprasad R, Hashim U, Gopinath SC, Kashif M, Veeradasan P, Balakrishnan S, Foo K, Poopalan P (2015) Low temperature annealed zinc oxide nanostructured thin film-based transducers: characterization for sensing applications. PLoS One 10:e0132755

Holmen LG, Haakestad MW (2016) Optical limiting properties and z-scan measurements of carbon disulfide at 2.05 μm wavelength. JOSA B 33:1655–1660

Kasi GK, Dollahon NR, Ahmadi TS (2007) Fabrication and characterization of solid PbI2 nanocrystals. J Phys D 40:1778

Kenyon A (2002) Recent developments in rare-earth doped materials for optoelectronics. Prog Quantum Electron 26:225–284

Khan MT, Almohammedi A (2017) Effect of CdS nanocrystals on charge transport mechanism in poly (3-hexylthiophene). J Appl Phys 122:075502

Khan MT, Kaur A, Dhawan S, Chand S (2011) Hole transport mechanism in organic/inorganic hybrid system based on in-situ grown cadmium telluride nanocrystals in poly (3-hexylthiophene). J Appl Phys 109:114509

Kim M-S, Yim K-G, Son J-S, Leem J-Y (2012) Effects of Al concentration on structural and optical properties of Al-doped ZnO thin films. Bull Korean Chem Soc 33:1235–1241

Kumar S, Sahare P (2012) Nd-doped ZnO as a multifunctional nanomaterial. J Rare Earths 30:761–768

Kumar V, Ntwaeaborwa O, Soga T, Dutta V, Swart H (2017) Rare earth doped zinc oxide nanophosphor powder: a future material for solid state lighting and solar cells. ACS Photonics 4:2613–2637

Lan C, Dong R, Zhou Z, Shu L, Li D, Yip S, Ho JC (2017) Large-scale synthesis of freestanding layer-structured PbI2 and MAPbI3 nanosheets for high-performance photodetection. Adv Mater 29:1702759

Lian H, Hou Z, Shang M, Geng D, Zhang Y, Lin J (2013) Rare earth ions doped phosphors for improving efficiencies of solar cells. Energy 57:270–283

Liu Y, Luo W, Li R, Zhu H, Chen X (2009) Near-infrared luminescence of Nd 3 + and Tm 3 + ions doped ZnO nanocrystals. Optics express 17:9748–9753

Liu J, Liang Z, Xu B, Xiang H, Xia Y, Yin J, Liu Z (2016) Synthesis of PbI 2 nanowires for high sensitivity photodetectors. RSC Adv 6:59445–59449

Madhi I, Bouzid B, Bessaïs B (2016) Effect of annealing temperature and Sn doping on structural, morphological and NO2 detection properties of nanostructured ZnO thin films. Sens Lett 14:389–395

Mesquita I, Andrade L, Mendes A (2017) Perovskite solar cells: materials, configurations and stability. Renew Sustain Energy Rev 80:2471–2489

Moazzami R, Hu C, Shepherd WH (1992) Electrical characteristics of ferroelectric PZT thin films for DRAM applications. IEEE Trans Electron Devices 39:2044–2049

Mohd S, Khan ZR, Hamdy MS, Algarni H, AlFaify S (2018) A facile microwave-assisted synthesis of PbMoO 4 nanoparticles and their key characteristics analysis: a good contender for photocatalytic applications. Materials Res Express 5:095032

Mousa AM, Al-rubaie NJ (2011) Properties of layered PbI2 doped with Al and Co. J Materials Sci Eng 5:32

Mulato M, Lu J, Street R (2001) Simulated and measured data-line parasitic capacitance of amorphous silicon large-area image sensor arrays. J Appl Phys 89:638–647

Ono LK, Qi Y, Liu SF (2018) Progress toward stable lead halide perovskite solar cells. Joule 2:1961–1990

Panda D, Tseng T-Y (2013) Growth, dielectric properties, and memory device applications of ZrO2 thin films. Thin Solid Films 531:1–20

Poornesh P, Hegde PK, Umesh G, Manjunatha M, Manjunatha K, Adhikari A (2010) Nonlinear optical and optical power limiting studies on a new thiophene-based conjugated polymer in solution and solid PMMA matrix. Opt Laser Technol 42:230–236

Rani TD, Tamilarasan K, Elangovan E, Leela S, Ramamurthi K, Thangaraj K, Himcinschi C, Trenkmann I, SchuIze S, Hietschold M (2015) Structural and optical studies on Nd doped ZnO thin films. Superlattices Microstruct 77:325–332

Ren W, Trolier-McKinstry S, Randall CA, Shrout TR (2000) Bismuth zinc niobate pyrochlore dielectric thin films for capacitive applications. J Appl Phys 89:767–774

Rinnert H, Miska P, Vergnat M, Schmerber G, Colis S, Dinia A, Muller D, Ferblantier G, Slaoui A (2012) Photoluminescence of Nd-doped SnO2 thin films. Appl Phys Lett 100:101908

Rybak O (2014) Growth and properties of Cu-and Ag-Doped PbI2 crystals. Inorg Mater 50:205–208

Rybak O, Lun YO, Bordun I, Omelyan M (2005) Crystal growth and properties of PbI 2 doped with Fe and Ni. Inorg Mater 41:1124–1127

Salado M, Jodlowski AD, Roldan-Carmona C, de Miguel G, Kazim S, Nazeeruddin MK, Ahmad S (2018) Surface passivation of perovskite layers using heterocyclic halides: improved photovoltaic properties and intrinsic stability. Nano Energy 50:220–228

Saliba M (2018) Perovskite solar cells must come of age. Science 359:388–389

Saliba M, Correa-Baena JP, Grätzel M, Hagfeldt A, Abate A (2018) Perovskite solar cells: from the atomic level to film quality and device performance. Angew Chem Int Ed 57:2554–2569

Satpal SB, Athawale AA (2018) Synthesis of ZnO and Nd doped ZnO polyscales for removal of rhodamine 6G dye under UV light irradiation. Materials Res Express 5:085501

Sears WM, Klein M, Morrison J (1979) Polytypism and the vibrational properties of Pb I 2. Phys Rev B 19:2305

Shide W, Chao L, Wei W, Huanxin W, Yanliang S, Youqi Z (2010) Nd-doped SnO2: characterization and its gas sensing property. J Rare Earths 28:171–173

Shkir M, AlFaify S (2017) Tailoring the structural, morphological, optical and dielectric properties of lead iodide through Nd3 + doping. Sci Rep 7:16091

Shkir M, Kilany M, Yahia IS (2017a) Facile microwave-assisted synthesis of tungsten-doped hydroxyapatite nanorods: a systematic structural, morphological, dielectric, radiation and microbial activity studies. Ceram Int 43:14923–14931

Shkir M, Ganesh V, AlFaify S, Yahia IS (2017b) Structural, linear and third order nonlinear optical properties of drop casting deposited high quality nanocrystalline phenol red thin films. J Mater Sci 28:10573–10581

Shkir M, AlFaify S, Yahia IS, Hamdy MS, Ganesh V, Algarni H (2017c) Facile hydrothermal synthesis and characterization of cesium-doped PbI2 nanostructures for optoelectronic, radiation detection and photocatalytic applications. J Nanopart Res 19:328

Shkir M, Ganesh V, Yahia I, AlFaify S (2018a) Microwave-synthesis of La 3 + doped PbI 2 nanosheets (NSs) and their characterizations for optoelectronic applications. J Mater Sci 29:15838–15846

Shkir M, Taukeer Khan M, Ganesh V, Yahia IS, Ul Haq B, Almohammedi A, Patil PS, Maidur SR, AlFaify S (2018b) Influence of Dy doping on key linear, nonlinear and optical limiting characteristics of SnO2 films for optoelectronic and laser applications. Opt Laser Technol 108:609–618

Shkir M, Yahia IS, Ganesh V, Bitla Y, Ashraf IM, Kaushik A, AlFaify S (2018c) A facile synthesis of Au-nanoparticles decorated PbI2 single crystalline nanosheets for optoelectronic device applications. Sci Rep 8:13806

Shkir M, Yahia IS, Kilany M, Abutalib MM, AlFaify S, Darwish R (2019) Facile nanorods synthesis of KI:HAp and their structure-morphology, vibrational and bioactivity analyses for biomedical applications, Ceramics Int, ;45:50–55 https://doi.org/10.1016/j.ceramint.2018.09.132(2018)

Street R, Ready S, Van Schuylenbergh K, Ho J, Boyce J, Nylen P, Shah K, Melekhov L, Hermon H (2002) Comparison of PbI2 and HgI2 for direct detection active matrix X-ray image sensors. J Appl Phys 91:3345–3355

Tan M, Hu C, Lan Y, Khan J, Deng H, Yang X, Wang P, Yu X, Lai J, Song H (2017) 2D Lead Dihalides for high-performance ultraviolet photodetectors and their detection mechanism investigation, Small, 13:1702024

Taukeer Khan M, Kaur A, Dhawan S, Chand S (2011) In-situ growth of cadmium telluride nanocrystals in poly (3-hexylthiophene) matrix for photovoltaic application. J Appl Phys 110:044509

Tutt LW, Kost A (1992) Optical limiting performance of C60 and C70 solutions. Nature 356:225

Usha K, Sivakumar R, Sanjeeviraja C (2013) Optical constants and dispersion energy parameters of NiO thin films prepared by radio frequency magnetron sputtering technique. J Appl Phys 114:123501

Wang Y, Gan L, Chen J, Yang R, Zhai T (2017) Achieving highly uniform two-dimensional PbI2 flakes for photodetectors via space confined physical vapor deposition. Sci Bull 62:1654–1662

Wangyang P, Sun H, Zhu X, Yang D, Gao X (2016) Mechanical exfoliation and Raman spectra of ultrathin PbI2 single crystal. Mater Lett 168:68–71

Woo T, Kim T (2012) Light collection enhancement of the digital X-ray detector using Gd2O2S: Tb and CsI: Tl phosphors in the aspect of nano-scale light dispersions. Radiat Phys Chem 81:12–15

Wood GL, Clark WW, Miller MJ, Salamo GJ, Sharp EJ (1989) Evaluation of passive optical limiters and switches. In: Proceedings of the SPIE 1105, materials for optical switches, isolators, and limiters, vol 1105, pp 154–181

Yu K, Qiu X, Xu X, Wei W, Peng B, Zhou Z (2007) Enhanced photoluminescence of Nd 2 O 3 nanoparticles modified with silane-coupling agent: Fluorescent resonance energy transfer analysis. Appl Phys Lett 90:091916

Zhang Q, Huang X (2010) Recent progress in quantum cutting phosphors. Prog Materials Sci 55:353–427

Zheng W, Zhang Z, Lin R, Xu K, He J, Huang F (2016) High-crystalline 2D layered PbI2 with ultrasmooth surface: liquid-phase synthesis and application of high-speed photon detection. Adv Electron Materials 2:1600291

Zhong M, Huang L, Deng H-X, Wang X, Li B, Wei Z, Li J (2016) Flexible photodetectors based on phase dependent PbI 2 single crystals. J Materials Chem C 4:6492–6499

Zhu X, Wei Z, Jin Y, Xiang A (2007) Growth and characterization of a PbI2 single crystal used for gamma ray detectors. Cryst Res Technol 42:456–459